LOW-TEMPERATURE FAR-INFRARED ELLIPSOMETRY OF CONVERGENT BEAM

A. B. Sushkov[†] and E. A. Tishchenko

*P.L.Kapitza Institute for Physical Problems, Russian Academy of Science,
Kosygina str. 2, 117973 Moscow, Russia*

*[†]Institute of Spectroscopy, Russian Academy of Science,
142092 Troitsk, Moscow region, Russia*

Development of an ellipsometry to the case of a coherent far infrared irradiation, low temperatures and small samples is described, including a decision of the direct and inverse problems of the convergent beam ellipsometry for an arbitrary wavelength, measurement technique and a compensating orientation of cryostat windows. Experimental results are presented: for a gold film and UBe_{13} single crystal at room temperature (λ=119 μm), temperature dependencies of the complex dielectric function of $SrTiO_3$ (λ=119, 84 and 28 μm) and of $YBa_2Cu_3O_{7-\delta}$ ceramic (λ=119 μm).

Key words: ellipsometry, far infrared, convergent beam, inverse problem.

1. Introduction

Ellipsometry is a well known technique[1,2] of measurement of the optical constants of different substances. Despite of being known from the beginning of the century, ellipsometry has begun to develop intensively only together with lasers and computers. Work[3] is one of the few early attempts to develop ellipsometry into far infrared. Recent years heavy Fermion systems and, especially, high-T_C superconductors has given a rise to the new efforts in the far infrared ellipsometry[4,5]. In this paper we describe our method, ellipsometer and some experimental results.

2. Far-infrared ellipsometry on small samples

2.1 Parallel or convergent beam?

Far infrared is characterized by significant divergency of the beams due to the value of λ/d ratio, where λ is a wavelength and d is a beam diameter. It means, that it is impossible to create a thin parallel beam of far infrared as it is possible in visible. Thus, there are two alternative approaches to the far infrared ellipsometry on the small samples:
1) the sample is in a wide parallel beam the electromagnetic field is of nonzero value on the edges of the sample, reflection and diffraction parts of the field are detected;
2) the sample is placed in the focus of a lens or a mirror the field on the edges of the sample can be put equal to zero and diffraction effects may be neglected.

Both these approaches suggest appropriate calculations of diffraction effects in the former and of the convergency of the beam in the latter case. In the case of a wide parallel beam diffraction field can be introduced in the parabolic-equation approximation of the scalar theory of diffraction as parabolic-like half-shadow zones from each edge of the sample[6]. At large angles of incidence (80°) these zones will be essentially inter-mixed just near the far edge of the sample, so the detected field will contain a diffraction part. Scalar theory of diffraction is not the sufficient one for the ellipsometry. This case the decision of the problem of a polarized plane wave diffraction on the impedance edge should be used. We suggest that such a decision can depend on the curvature radius of the edge as parameter, which is always unknown value in the experiment. That item needs a separate experimental study. Unfortunately, our sample holders ab initio were designed for the convergent beam geometry and do not allow us to carry out such a study.

Is that diffraction effect from the edges a negligible one? To our opinion, that effect can be neglected only in the case of the low reflected samples. In the case of highly reflected samples the diffraction effect of the edges can be of the order of the small reflection effect to be measured. For example, gold mirror[7,8] at λ=100 μm and 80° due to reflection produces Δ_{ps}=1.17° and Ψ=44.65°, where as usual $\rho = \tan\Psi\,exp(i\Delta)$. We have chosen a convergent beam (CB) ellipsometry. In the case of CB-ellipsometry we reduce to a minimum value the diffraction effects, but the problem of a correct account of the convergent beam reflection arises. We have found
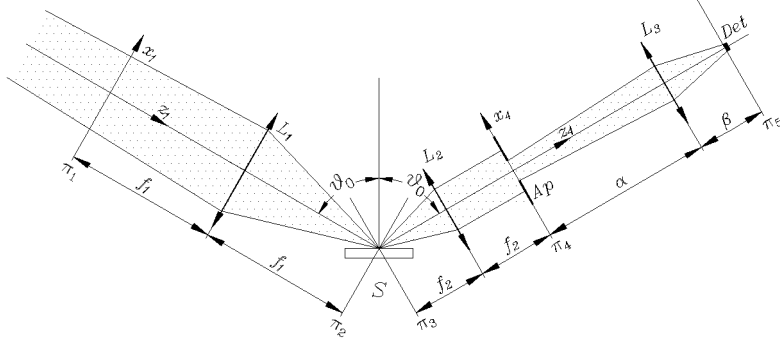
Fig. 1. Optical scheme of the convergent-beam ellipsometer for far infrared: L_1, L_2, L_3—lenses with focal lengths f_1, f_2, f_3, respectively; S—sample; Det—detector; $\pi_1 - \pi_5$— fundamental planes; θ_0—angle of incidence of the beam; the optimal position of polarizer and analyzer is between lenses L_1 and L_2; and $1/\alpha + 1/\beta = 1/f_3$.

the decision of the direct problem of the CB ellipsometry, quite adequate to the experimental problems.

2.1 Convergent beam ellipsometry

The direct problem of the convergent beam ellipsometry is to calculate the detected signal in terms of the reflection matrix of the sample and the field distribution in the beam. Our decision[4] is based on the lens's Fourier-transform capability[9]. That decision simultaneously determines the optical scheme of the CB-ellipsometer (Fig. 1). Let's designate $E_{x_1}(x_1, y_1)$ and $E_{y_1}(x_1, y_1)$ the complex amplitudes of x- and y-polarized beams in the input plane π_1, then the field in the output plane π_4 is:

$$\left[\begin{array}{c} E_{x_4} \\ E_{y_4} \end{array} \right] (x_4, y_4) = \mathbf{R}_C(x_4, y_4) \left[\begin{array}{c} E_{x_1} \\ E_{y_1} \end{array} \right] (x_4 f_1/f_2, -y_4 f_1/f_2), \qquad (1)$$

where $\mathbf{R}_C$ is modified reflection matrix. It can be found in coordinates (θ, φ), where θ is the angle of incidence of a partial plane wave in its own plane of incidence and φ is the azimuth of this plane

$$\mathbf{R}_C(\theta, \varphi) = \mathbf{A}_L \mathbf{R}(\theta, \varphi) \, \mathbf{A}_R(\theta, \varphi) \qquad (2)$$

where

$$\mathbf{R} = \left[\begin{array}{cc} R_{pp} & R_{ps} \\ R_{sp} & R_{ss} \end{array} \right] - \qquad (3)$$

3

is a reflection matrix of a general kind[1] for a partial plane wave, and

$$\mathbf{A}_L = \begin{bmatrix} a & -b \\ -c & d \end{bmatrix}, \qquad \mathbf{A}_R = \frac{1}{ad - bc} \begin{bmatrix} d & -b \\ -c & a \end{bmatrix}, \qquad (4)$$

$$\begin{cases} a &= \cos(\theta_0)\cos(\theta)\cos(\varphi) + \sin(\theta_0)\sin(\theta) \\ b &= -\cos(\theta_0)\sin(\varphi) \\ c &= \cos(\theta)\sin(\varphi) \\ d &= \cos(\varphi) \end{cases} \qquad (5)$$

To calculate $\mathbf{R}_C$ - matrix in $(x4, y4)$ coordinates, the variables are to be changed:

$$\begin{cases} \cos(\theta) = \left\{ x_4 \sin(\theta_0) + \cos(\theta_0)\sqrt{f_2^2 - x_4^2 - y_4^2} \right\} / f_2 \\ \tan(\varphi) = y_4 / \left\{ \sin(\theta_0)\sqrt{f_2^2 - x_4^2 - y_4^2} - x_4 \cos(\theta_0) \right\} \end{cases} \qquad (6)$$

Placing an aperture in the output plane π_4 we can filtrate some part of the output field, corresponding to the part of reflected plane waves. Lens L_3 creates the image of the aperture in the detector plane π_5. Detected signal in the ideal ellipsometer can be written as:

$$I_D(A) \propto \iint_{Ap} \{ E_{x_4}(x_4, y_4)\cos(A) + E_{y_4}(x_4, y_4)\sin(A) \} \{\ldots\}^* \, dx_4 \, dy_4 \quad (7)$$

where A — angle of analyzer, $\{\ldots\}^*$ means complex conjugation and the integral is to be taken over the aperture Ap in the plane π_4. To compare the detected signal in the case of the convergent beam to that one in the case of the alone plane wave expression (7) should be rewritten:

$$I_D(A) \propto I_{xx} \cos^2(A) + I_{xy}\sin(A)\cos(A) + I_{yy}\sin^2(A) \qquad (8)$$

In the case of alone plane wave the detected signal has the same appearance as (7) with the following differences:

$$\text{convergent beam:} \quad \begin{cases} I_{xx} = \iint_{Ap} E_{x_4} E_{x_4}^* \, dx_4 \, dy_4 \\ I_{xy} = \iint_{Ap} (E_{x_4} E_{y_4}^* + E_{x_4}^* E_{y_4}) \, dx_4 \, dy_4 \\ I_{yy} = \iint_{Ap} E_{y_4} E_{y_4}^* \, dx_4 \, dy_4 \end{cases} \qquad (9)$$

$$\text{plane wave:} \quad \begin{cases} I_{xx} = E_{x_4} E_{x_4}^* \\ I_{xy} = E_{x_4} E_{y_4}^* + E_{x_4}^* E_{y_4} \\ I_{yy} = E_{y_4} E_{y_4}^* \end{cases} \qquad (10)$$

If a sample is an ideal mirror, expressions (9) coincide with (10) ones. In the opposite case, each point of the output plane π_4 has its own polarization ellipse and averaged coefficients (9) should be computed.

In addition to the quantitative results above two qualitative notices can be done.
a) The convergency of the beam will affect mainly on the averaged ellipticity of the beam.
b) No matter in what point between the lenses L_1 and L_2, together consisting a telescope, the reflecting sample is placed.

2.2 Possibility of Multiple-Angle-of-Incidence (MAI) ellipsometry

Optical scheme of the CB-ellipsometer (Fig. 1) contains an interesting opportunity of MAI measurements. To carry out MAI measurements someone should move the output aperture Ap in the plane π_4 in x-direction perpendicularly to the optical axis. MAI ellipsometry can be used to determine the thickness of the film to be investigated. We checked such opportunity on pure substrate of $SrTiO_3$. Some of results are in Fig. 2. Parameter χ follows to the model computation line, while parameter γ deflects from it's line appreciably. Parameter γ is mainly connected with a phase shift. It points out to the phase distribution in a real beam as a possible reason for that deflection. So, we can't use that simple scheme for MAI ellipsometry, although measurements at different central angles of incidence give more close results[4]. We suggest that measurements with uncoherent light can give better results.

3. Ellipsometric technique

3.1 Ellipsometric scheme

We have chosen compensatorless scheme of the ellipsometer to simplify experiment, to work in a wide spectral region, and to avoid additional difficulties in solving the direct problem of CB-ellipsometry. We measure two parameters of the polarization ellipse - azimuth χ and ellipticity γ - both averaged over the aperture. Experimentally measured values are analyzer angle A_{min}, at which the detected signal is of minimal value and relation of the minimal signal to the maximal one:

$$\chi = A_{min} \tag{11}$$

$$\tan^2(\gamma) = I_D(A_{min})/I_D(A_{min} \pm \pi/2) \tag{12}$$

These values can also be computed from (8), (9). Equating the first derivative of the detector signal (8) to zero, someone obtains:

$$A_{ext1} = \frac{1}{2}\arctan(\frac{I_{xy}}{I_{xx} - I_{yy}}) \tag{13}$$

$$A_{ext2} = A_{ext1} \pm \pi/2 \tag{14}$$

where A_{ext1} and A_{ext2} are extrema of the function $I_D(A)$, one of those is minimum, another — maximum. In any case, to use (12) the function (8) should be computed at both points (13) and (14). Computer program can readily distinguish which one is minimum and vise versa. Thus, we can as measure as calculate two parameters: averaged azimuth χ and averaged ellipticity γ, that permits to decide the inverse problem.

3.2 Inverse problem

In brief, the numerical inversion problem is to find such values of parameters of the reflecting system, that error function F has a minimum value[1]. For the multiple-angle-of-incidence (MAI) technique let us define the error function F as follows:

$$F = \sum_{i=1}^{M} \left\{ (\chi_i^m - \chi_i^c)^2 + (\gamma_i^m - \gamma_i^c)^2 \right\} \tag{15}$$

where M is the number of measurements (the number of incidence angles), χ_i^m and γ_i^m denotes angles from the ith measurement, χ_i^c and γ_i^c are computed values. In this paper only a simplest reflecting system — an isotropic semi space — is discussed. In that case F is a function of two variables, e.g. n and κ — refraction and extinction coefficients of the substance. It's necessary to study the surface of $F(n, \kappa)$ to draw the conclusion about existing of the single minimum of this function.

Let's take SrTiO$_3$ single crystal as probe material, because of its large optical constants in far infrared, cubic structure and wide use as a substrate for YBaCuO films. Results of a simple computer experiment are in Fig. 3. Let's take the computed for the convergent beam values χ^m and γ^m as
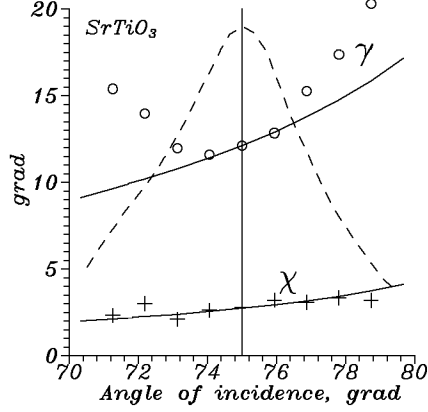
Fig. 2. Ellipsometric parameters χ and γ vs a shift of a 6×40 mm slit in the plane π_4 of Fig. 1; crosses and circles — experiment, solid lines — computation, dashed line — intensity of the beam at s-polarization.
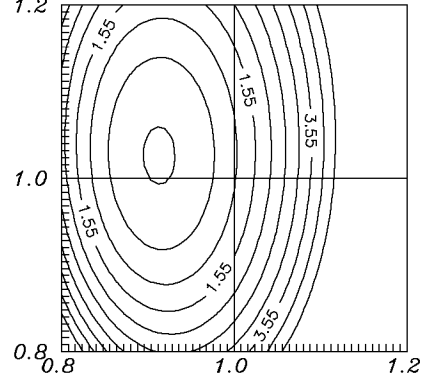
Fig. 3. Contour map of the error function $F(n,\kappa)$ at n=22, κ=13, λ=119 μm, M=1, θ_0=80°, aperture of diameter 30 mm, L_1=L_2=153 mm.

measured ones, but $\chi^c(n,\kappa)$ and $\gamma^c(n,\kappa)$ we will calculate for the plane

wave. This is a model of a convergent beam experiment with a plane wave treatment. Two conclusions can be drawn from Fig. 3:

i) the error function $F(n,\kappa)$ has a single minimum, so the inverse problem has a single decision;

ii) the displacement of the minimum illustrates the influence of the focusing of the far infrared beam or difference between two approximations: of the plane wave and of the convergent beam.

Comparing $\chi = 11.18°$, $\gamma = 7.02°$, computed for the convergent beam, to $\chi = 11.19°$, $\gamma = 5.88°$, computed for the plane wave, we can draw the third conclusion:

iii) the convergency of a beam influences on value of γ and practically does not influence on value of χ.

3.3 Problem of cryostat windows

In a general case window is a thick anisotropic plate. In the case of a convergent beam windows must be *thin*. It means that 1-st, 2-nd, ..., ith convergent beams, reflected inside window plate, all must have the same focal point. Because of this reason, due to its transparency in visible and far infrared and also due to its low temperature properties we use 20 μm mylar as material both for warm and cold windows. Mylar is

known to be an anisotropic material in far infrared[10]. Rotating 20 μm mylar foil between crossed polarizer and analyzer ($P\perp A$) we detected two approximately perpendicular axises of zero effect to the polarization of the beam. Maximum signal in that experiment was 8×10^{-4} of the signal in $P\|A$ orientation at λ=119 μm. Black polyethylene shows 1.4×10^{-3} at λ=84 μm. Being mounted in an arbitrary orientation 4 windows and 2 filters can give a significant polarization effect. We proposed following minimization and account of this effect.

According to our development above, in presence of the windows, matrix $\mathbf{R}_C(x_4, y_4)$ in equation (1) should be modified:

$$\mathbf{R}_C(x_4, y_4) \Rightarrow T_4(x_4, y_4)\, T_3(x_4, y_4)\, \mathbf{R}_C(x_4, y_4)\, T_2(x_4, y_4)\, T_1(x_4, y_4) \quad (16)$$

where $T_i(x_4, y_4)$ is 2×2 matrix of each window for every partial plane wave. But a strict account of the windows is practically impossible because we deal with the not normal incidence of a convergent beam onto a concave or convex anisotropic film with an unknown model of anisotropy. We prefer to minimize the windows anisotropy effect by their compensating orientation as it is described in Appendix and measure the rest of the effect due to the not normal incidence of the beam as a complex constant T_W, describing the transmission of all for windows. This value is used in solving of the inverse problem for the cold measurements.

4. Experiment

4.1 Setup

According to the optical scheme of Fig. 1, far infrared ellipsometer was made up with water vapor electro-discharged laser being the source and liquid helium cooled photo-resistors Ge:Ga, Si:B, GaAS as the far infrared detectors. The section of the setup by plane of incidence is shown in Fig. 4c. All lenses are made up of polyethylene. Both polarizer and analyzer consist of two sheets: i) alumina film stripes on thephlon replica with .8 μm period and ii) metal mesh with periods 20×400 μm. Polarizers should be placed as close to the sample as possible to minimize polarization inhomogeneity of the beam due to that one of the optical elements, including polarizer and analyzer. The sample is in the atmosphere of a cryoagent. To filtrate

a) Block–scheme

b) Orientation of mylar windows
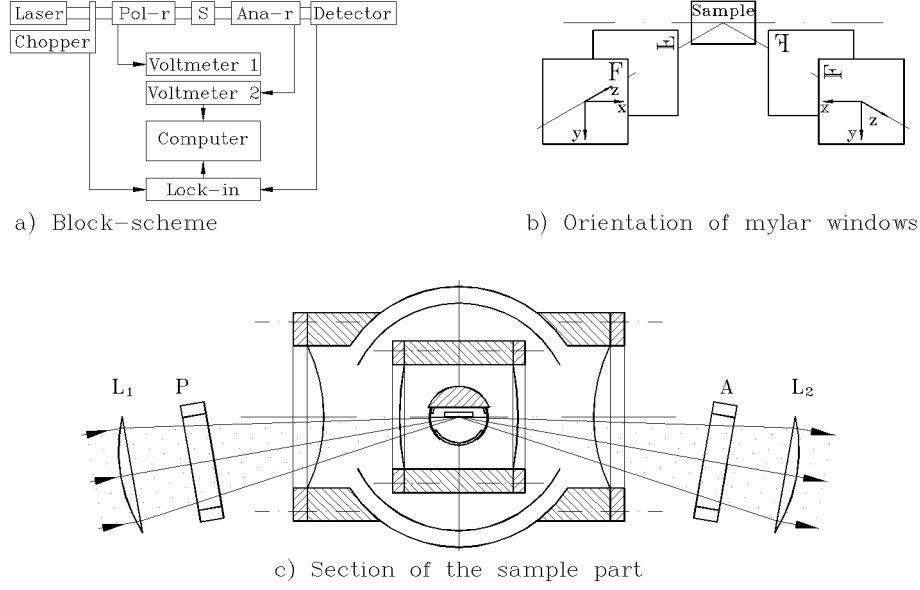
c) Section of the sample part

Fig. 4. Setup.

the short wavelength irradiation a black polyethylene (in compensating orientation) surrounds the sample.

Block-scheme of the setup is in Fig. 4a. By means of precision multi-revolution potentiometers P- and A-angles are transformed to the voltage. Accuracy and linearity of this transformation both are of order $\pm 0.1°$. To measure an intensity of light a lock-in technique at modulation frequency 80 Hz is used. The polarizer is at fixed angle $\pm 45°$, the analyzer is rotated near the minimum of intensity and this part of the curve $I_D(A)$ is recorded in the computer file. A_{min} and $I_D(A_{min})$ are calculated and analyzer begins to rotate to the A_{max} angle. A linearity range of the detector does not exceed 10^2, but we need to measure values of I_{max}/I_{min} of order 10^4 for the metallic samples. So we use paper sheets as attenuators (each of order 3 at 119 μm) to measure the signal at the same gain of the lock-in amplifier. Such measurement routine requires a time stability of the laser irradiation.

The time instability of irradiation and the small movements of the sample in the cooling process (up to 0.3 mm) are two main sources of random errors. The whole cryostat is mounted on the movable optical

9

table to adjust the sample in x-direction. Errors due to the beginning of cooling process are good seen in the upper curves in Fig. 5.

4.1.1 Room temperature results

Some experimental results are presented in the Table to illustrate the sensitivity of the ellipsometer. All these results were obtained at room temperature, at λ=119 μm without windows. Expected values for gold[7,8] are $\chi = 45° - 0.36°$ and $\tan^2(\gamma) = 9.64 \times 10^{-5}$. As can be seen from a transmittance measurements, accuracy of the ellipsometer is sufficient for gold's measurements. Increasing value of ellipticity γ, corresponding mainly to the phase shift, can be caused by uncertainties of the surface of the gold film. For UBe$_{13}$ we have computed $W_p = 14600$ cm^{-1} and $W_\tau = 670$ cm^{-1}. Computed from these values free electrons's concentration $(m_e = 1)$ $N_e = 2.35 \times 10^{21}$ is in good agreement with that one from Hall-effect measurements[11].

Sample	Measr. values	Polarizer angle, P			
		$-45°$	$0°$	$+45°$	$+90°$
No sample, transm.	χ	$+0.13°$	$+0.25°$	$-0.10°$	$0°$
	$\tan^2(\gamma)$	5×10^{-6}	5×10^{-6}	5×10^{-6}	5×10^{-6}
Au film	χ	$+0.39°$	$-0.01°$	$-0.60°$	$0°$
	$\tan^2(\gamma)$	4.14×10^{-4}	9×10^{-6}	6.28×10^{-4}	7×10^{-6}
UBe$_{13}$ single cr.	χ	$+3.53°$		$-3.41°$	
	$\tan^2(\gamma)$	4.74×10^{-3}		4.53×10^{-3}	

4.2 Results of SrTiO$_3$ measurements

Temperature dependencies of real and imaginary parts of the complex dielectric function of SrTiO$_3$ single crystal are shown in Fig. 5. Such kind of behavior is caused by softening of low-frequency mode, centered between 80 – 90 cm^{-1}. We have measured different samples from independent sources and obtained different optical constants, especially at the frequency 84 cm^{-1}. Re-polishing of the samples does not change their optical constants. In literature[12–14] low-frequency constants also different. We suggest that
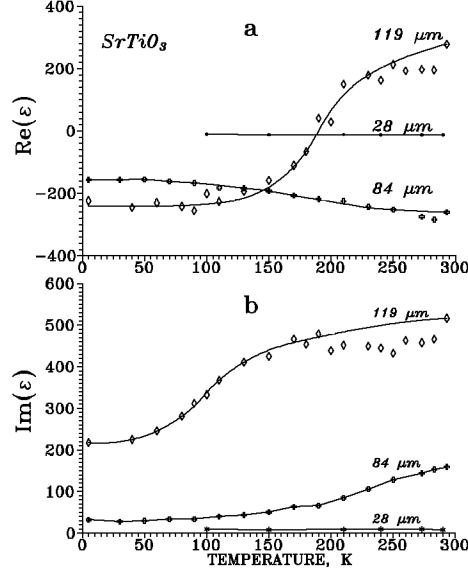
10

Fig. 5. Temperature dependence of the complex dielectric function of SrTiO$_3$ single crystal at 3 wavelengths.
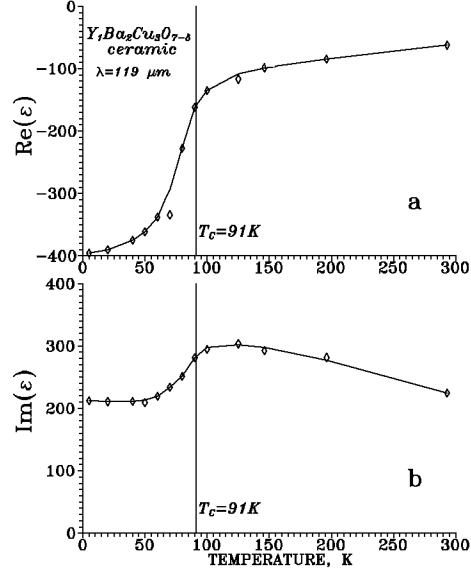
Fig. 6. Temperature dependence of the complex dielectric function of YBaCuO ceramic at wavelength 119 μm.

the lowest frequency mode is very sensitive to the quality of SrTiO$_3$ single crystals.

4.3 Superconductive transition in YBaCuO ceramic

Temperature dependence of the complex dielectric function of 1-2-3 ceramics at wavelength 119 μm is shown in Fig. 6. Sintered on air and annealed in oxygen atmosphere sample was polished with diamond paste. The behavior of the complex dielectric function is determined by chaotically oriented small crystals with different optical constants for $a-$, $b-$, and $c-$axis. Porous structure of the surface of the ceramics also effects on the measured values of the complex dielectric function.

5. Appendix

Let 2×2 matrix $\mathbf{T}$ describes the transmittance of some window. Rotations of this window around the axes give the following results:

$$\text{Rotation } x \to y \quad \begin{bmatrix} 0 & 1 \\ -1 & 0 \end{bmatrix} \begin{bmatrix} t_{11} & t_{12} \\ t_{21} & t_{22} \end{bmatrix} \begin{bmatrix} 0 & -1 \\ 1 & 0 \end{bmatrix} = \begin{bmatrix} t_{22} & -t_{21} \\ -t_{12} & t_{11} \end{bmatrix} \quad (17)$$

$$\text{Rotation } y \to -y \quad \begin{bmatrix} 1 & 0 \\ 0 & -1 \end{bmatrix} \begin{bmatrix} t_{11} & t_{12} \\ t_{21} & t_{22} \end{bmatrix} \begin{bmatrix} 1 & 0 \\ 0 & -1 \end{bmatrix} = \begin{bmatrix} t_{11} & -t_{12} \\ -t_{21} & t_{22} \end{bmatrix} \quad (18)$$

$$\text{Rotation } x \to -x \quad \begin{bmatrix} -1 & 0 \\ 0 & 1 \end{bmatrix} \begin{bmatrix} t_{11} & t_{12} \\ t_{21} & t_{22} \end{bmatrix} \begin{bmatrix} -1 & 0 \\ 0 & 1 \end{bmatrix} = \begin{bmatrix} t_{11} & -t_{12} \\ -t_{21} & t_{22} \end{bmatrix} \quad (19)$$

Transmission of the first two windows W_1 and W_2 can be written as:

$$\mathbf{T}_{12} = \mathbf{T}_2 \mathbf{T}_1 = \begin{bmatrix} \tau_{11} & \tau_{12} \\ \tau_{21} & \tau_{22} \end{bmatrix} \begin{bmatrix} t_{11} & t_{12} \\ t_{21} & t_{22} \end{bmatrix} =$$

$$\begin{bmatrix} \tau_{11}t_{11} + \tau_{12}t_{21} & \tau_{11}t_{12} + \tau_{12}t_{22} \\ \tau_{21}t_{11} + \tau_{22}t_{21} & \tau_{21}t_{12} + \tau_{22}t_{22} \end{bmatrix} \quad (20)$$

If windows W_1 and W_2 are identical and W_2 is rotated then

$$\mathbf{T}_2 = \begin{bmatrix} \tau_{11} & \tau_{12} \\ \tau_{21} & \tau_{22} \end{bmatrix} = \begin{bmatrix} t_{22} & \pm t_{21} \\ \pm t_{12} & t_{11} \end{bmatrix} \quad (21)$$

and, putting the off-diagonal elements much less then the diagonal ones,

$$\mathbf{T}_{12} = \begin{bmatrix} t_{11}t_{22} \pm t_{21}^2 & t_{22}(t_{12} \pm t_{21}) \\ t_{11}(t_{21} \pm t_{12}) & t_{11}t_{22} \pm t_{12}^2 \end{bmatrix} \approx$$

$$t_{11}t_{22} \begin{bmatrix} 1 & (t_{12} \pm t_{21})/t_{11} \\ (t_{21} \pm t_{12})/t_{22} & 1 \end{bmatrix}, \quad (22)$$

where '+' means the presence and '−' means the absence of $(x \to -x)$ or $(y \to -y)$ rotations. So the values of the off-diagonal elements can be reduced to the minimum.

Let's now consider windows W_1 and W_2 as one window W_{12} and windows W_3 and W_4 as one window W_{34} (Fig. 3B). Then the reflection matrix $\mathbf{R}$ becomes:

$$\mathbf{R} \to \mathbf{W}_{34} \mathbf{R} \, \mathbf{W}_{12} = \begin{bmatrix} \tau_{11} & \tau_{12} \\ \tau_{21} & \tau_{22} \end{bmatrix} \begin{bmatrix} R_{pp} & R_{ps} \\ R_{sp} & R_{ss} \end{bmatrix} \begin{bmatrix} t_{11} & t_{12} \\ t_{21} & t_{22} \end{bmatrix} \approx$$

$$\begin{bmatrix} R_{pp}t_{11}\tau_{11} & R_{ps}t_{22}\tau_{11} + R_{pp}t_{12}\tau_{11} + R_{ss}t_{22}\tau_{12} \\ R_{sp}t_{11}\tau_{22} + R_{pp}t_{11}\tau_{21} + R_{ss}t_{21}\tau_{22} & R_{ss}t_{22}\tau_{22} \end{bmatrix} (23)$$

Due to the rotations (17),(18) matrix $\mathbf{W_{34}}$ should be changed according to (21) and the final expression for the reflection matrix between two windows can be written as follows:

$$\mathbf{W}_{34}\mathbf{R}\,\mathbf{W}_{12} = t_{11}t_{22}$$

$$\begin{bmatrix} R_{pp} & (R_{ps}t_{22} + R_{pp}t_{12} \pm R_{ss}t_{21})/t_{11} \\ (R_{sp}t_{11} \pm R_{pp}t_{12} + R_{ss}t_{21})/t_{22} & R_{ss} \end{bmatrix} \quad (24)$$

where, as usual, '+' means the presence and '−' means the absence of $(x \to -x)$ or $(y \to -y)$ rotations. So, practically full compensation of the cryostat windows effect can be reached.

6. Acknowledgments

7. References

1. R. M. Azzam and N. M. Bashara, "Ellipsometry and Polarized Light", North-Holland, Amsterdam, 1977.
2. A. V. Rjanov, K. K. Svitashev, A. I. Semenenko, L. V. Semenenko, V. K. Sokolov, "Osnovy ellipsometrii", Novosibirsk, 1979.
3. R. O. DeNicola, M. A. Saifi, and R. E. Frazee, "Epitaxial layer thickness measurement by far infrared ellipsometry", Appl. Opt., Vol. 11, No. 11, pp. 2534-2539, 1972.
4. A. B. Sushkov and E. A. Tishchenko, "Ellipsometry of a convergent beam in the far infrared", Optika i Spectroscopia, Vol. 72, No. 2, pp. 491-496, 1992, [Opt. Spectrosc. (USSR) Vol. 72, No. 2, pp. 265-268, 1992].
5. K.-L. Barth and F. Keilmann, "Far-infrared ellipsometer", Rev. Sci. Instrum., Vol. 64, No. 4, pp. 870-875, 1993.
6. L. A. Vainshtein, "Electromagnetic waves", Moscow, 1988.
7. G. Brandli and A. J. Sievers, "Absolute measurement of the far-infrared surface resistance of Pb", Phys. Rev. B, Vol. 5, No. 11, pp. 3550-3557, 1972.

8. M. A. Ordal, L. L. Long, R. J. Bell, S. E. Bell, R. R. Bell, R. W. Alexander,Jr., and C. A. Ward, "Optical properties of metals Al, Co, Cu, Au, Fe, Pb, Ni, Pd, Pt, Ag, Ti, and W in the infrared and far infrared ", Appl. Opt., Vol. 22, No. 7, pp. 1099-1119, 1983.

9. J. W. Goodman, "Introduction to Fourier Optics", McGrow-Hill, New-York, 1968.

10. D. R. Smith and E. V. Loewenstein, "Optical constants of far infrared materials. 3:plastics", Appl. Opt., Vol. 14, No. 6, p. 1335, 1975.

11. V. I. Nijankovskii, Dr. Sci. Dissertation, Institute for Physical problems, Moscow, 1990.

12. K. F. Pai, T. J. Parker, N. E. Tornberg, R. P. Lowndes, and W. G. Chambers, "Determination of the complex refractive indices of solids in the far infrared by dispersive Fourier transform spectroscopy II. Pseudo-displacive ferroelectrics", Infrared Phys., Vol. 18, No. 4, pp. 327-336, 1978.

13. J. C. Galzerani and R. S. Katiyar, "The infrared reflectivity in $SrTiO_3$ and the antidistortive transition", Solid State Commun., Vol. 41, No. 7, pp. 515-519, 1982.

14. V. N. Denisov, B. N. Mavrin, V. B. Podobedov, and J. F. Scott, "Hyper-Raman spectra and frequency dependence of soft mode damping in $SrTiO_3$", J. Raman Spect. Vol. 14, No. 4, pp. 276-283, 1983.